Figure S1

time window of *tcf21+* cell death and PAA compensation

A

Legend:
- *tcf21+* start dying
- *tcf21+* cells dead
- First compensating cells move into arches
- PAA3 re-formed
- PAA4 re-formed
- PAA5 re-formed
- PAA6 re-formed

time in hpf
32 36 40 44 48 52 56 60 64 68 72

alcian blue

96 hpf

B DMSO

C n=2

D Mtz

E n=3

flt1:YFP tcf21:mCherry-NTR

48 hpf	60 hpf	72 hpf	120 hpf
F DMSO	**G**	**H**	**I** n=1
J Mtz	**K**	**L**	**M** n=5

Figure S2

A

Exon 1   Exon2

Δ236 bp

100 bp

UTR   basic Domain   HLH Domain   coding sequence

B

beats/sec

3.0

2.5

2.0

1.5

wt   *tcf21-/-*   wt   *tcf21-/-*
48 hpf   72 hpf

wild type

C   D   n=2   E   n=4

tcf21-/-

F   G   n=6   H   n=7

alcian blue

96 hpf

tcf21:dsRed;
myl7:GFP

60 hpf

flk:GFP; tcf21:mCherry

I

Fraction of *tcf21*+ endothelial cells in PAA

1.0

0.5

0.0

wt nkx2.5 tcf21 nkx2.5; tcf21   wt nkx2.5 tcf21 nkx2.5; tcf21   wt nkx2.5 tcf21 nkx2.5; tcf21   wt nkx2.5 tcf21 nkx2.5; tcf21

PAA 3   PAA 4   PAA 5   PAA 6

Figure S3

overlay	*tcf21:mCherry*	*tie1*

wild type

nkx2.5-/-

tcf21-/-

nkx2.5-/- ; tcf21-/-

tcf21:mCherry; tie1

36 hpf
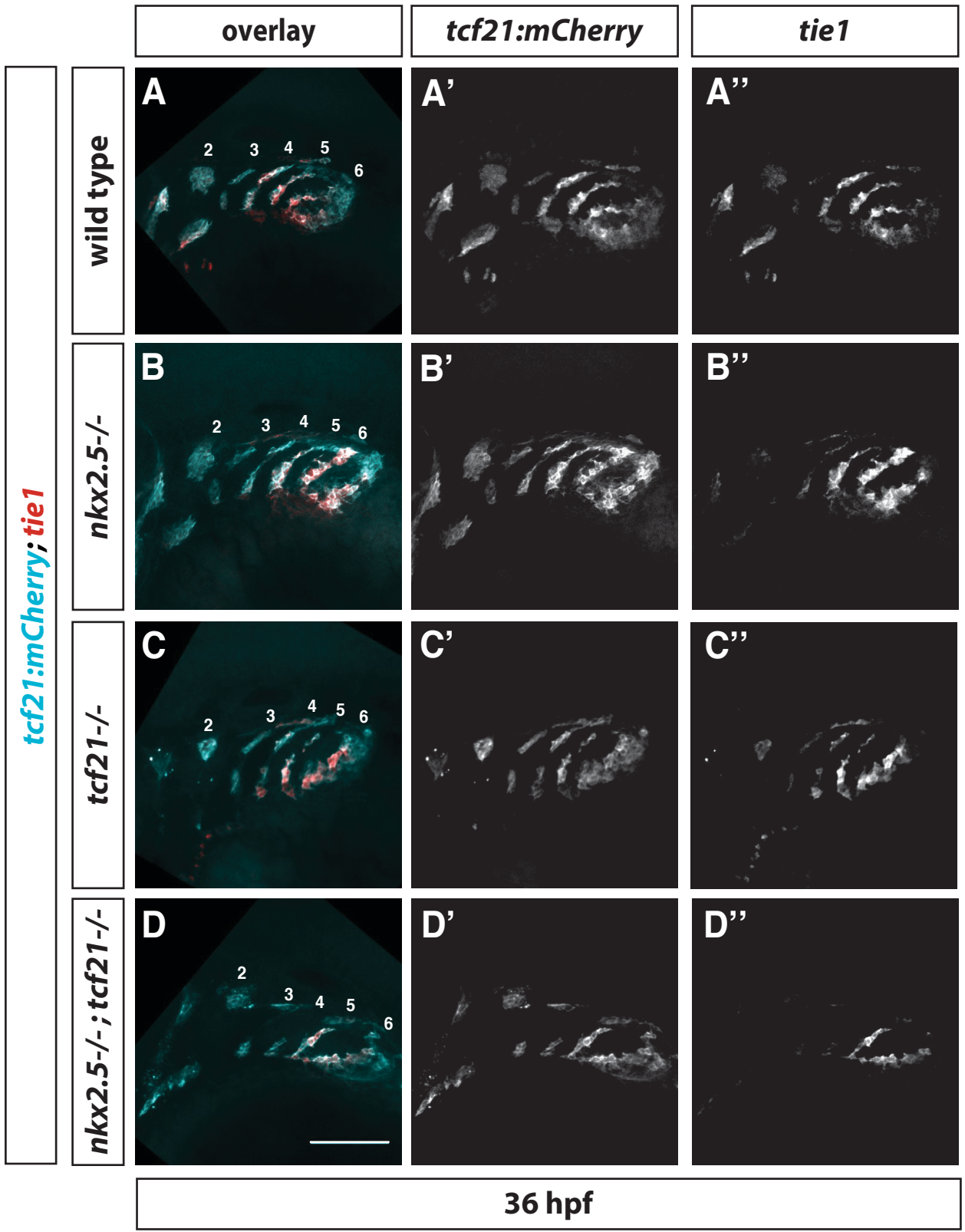
Figure S1, Related to Figure 3. pPAAs and cartilage form in the absence of tcf21+ cells.

(A) Graphical depiction of the time window in which *tcf21+* cells die in Mtz-treated *tcf21:mCherry-NTR; flk:GFP* embryos and of the time window in which the PAA 3-6 recover in Mtz-treated *tcf21:mCherry-NTR; flk:GFP* embryos. Gray lines are timelines and indicate the length (the beginning and the end) of the movies analyzed. The open brackets indicate the beginning of dying *tcf21+* cells and the beginning of the compensation (beginning of sprouting endothelial cells) in black and green, respectively. The closed brackets indicate the completion of *tcf21+* cell ablation and the completion of the connection of the compensating PAA3, 4, 5 or 6 from the LDA to the VA in black and light blue, dark blue, purple and red, respectively. Please note that brackets at the beginning of a timeline of a given movie indicate that the indicated process has started or finished but that the exact time of the indicated event is before the beginning of the movie.

(B-E) Alcian blue-stained embryo at 96 hpf without (B-C) or following (D-E) treatment with Mtz. While head size is reduced in *tcf21+* cell-ablated embryos, head cartilage still forms (D-E).

(F-M) Individual *flt1:YFP*; *tcf21:mCherry-NTR* embryos are followed from 48 to 120 hpf without (F-I) or following treatment with Mtz (J-M). In the control embryo, PAAs 3-6 form normally, though PAAs 3 and 4 are not labeled due to transgene variability which affects PAAs 3 and 4 in this transgenic line (F-I). In the Mtz-treated embryo, PAAs 3-6 are absent at 48 hpf following ablation (J), are remade

but partially lumenized at 60 and 72 hpf (K and L) and fully remade at 120 hpf
(M). Number of imaged embryos is indicated. Scale bars are 100 μm.

Figure S2, Related to Figure 4. Head cartilage forms and the overall heart morphology is not affected in the absence of *tcf21*.

(**A**) Schematic representing the *tcf21* genomic locus and the region deleted in the *tcf21* Δ236 mutant. Scale bar is 100 bp.

(**B**) Comparison of heart beat frequencies in wild-type and *tcf21* mutant embryos at indicated stages. n = 6 for all stages and genotypes. Individual data (grey dots), mean and SD are shown.

(**C-H**) Wild-type embryo (C-E) and *tcf21* mutant embryo (F-H) at indicated stages. Alcian blue staining indicates that the head cartilage still forms in *tcf21* mutant embryos (F, G) although the head size is reduced compared to wild-type embryos (C, D). The overall morphology of the heart is not affected in *tcf21* mutant embryo based on myocardium-specific GFP expression (E and H). Embryos shown in E and H were fixed in 4% PFA and imaged without further staining. Scale bars are 100 μm. Ventral views (C, E, F, H) and lateral views (D, G). n indicates the number of imaged embryos.

(**I**) Quantification of the contribution of *tcf21+* cells to PAAs 3 to 6 in wild-type (includes *tcf21-/+; nkx2.5-/+* and *tcf21-/+; nkx2.5-/+* embryos, n=12), *tcf21* mutant (includes *tcf21-/-; nkx2.5-/+* embryos, n=15), *nkx2.5* mutant (includes *nkx2.5-/-; tcf21-/+* embryos, n=13) and *tcf21; nkx2.5* double mutant embryos (n=4). Individual data points and the mean with the SEM are indicated. Note that using

mCherry expressed from the *tcf21* promoter is a less appropriate marker for labeling the pPAA progenitors compared to *nkx2.5:ZsYellow* (Figure 5Q) for two reasons. First, the perdurance of the mCherry in the pPAA progenitors is shorter leading to dimmer labeling of *tcf21+* cells, especially in the anterior pPAA 3, which is likely resulting from the differentiation of the PAAs in an anterior to posterior fashion. This may result in erroneous scoring of PAAs as having less pPAA progenitor contribution than seen when using *nkx2.5:ZsYellow* as a pPAA progenitor marker. Second, a specific subpopulation of anterior and ventral endothelial cells in the LDA express *tcf21*. Therefore, compensating endothelial cells from the LDA may be scored as *tcf21+* although they do not represent pPAA progenitors. This is not the case for compensating cells from the PHS, which do not express *tcf21*. However, as *nkx:ZsYellow* is not expressed in either the LDA or PHS, this is likely to account for differences seen when comparing results using *tcf21:mCherry-NTR* versus *nkx2.5:ZsYellow* as a marker for pPAA progenitors.

Figure S3, Related to Figure 5. Efficient specification of pPAA progenitors requires the combined activity of Tcf21 and Nkx2.5.

(**A-D**) 36 hpf *tcf21:mCherry-NTR* embryos of indicated genotypes stained for *tie1* mRNA (red) and mCherry (cyan) expression. The mCherry and *tie1* fluorescent signals are shown separately in A'-D' and A''-D'', respectively. Numbers in A-D indicate the pharyngeal arches 2-6. Note that the *tcf21+* cells in the first two pharyngeal arches are dying in embryos without Tcf21 function. Anterior is to the

left and dorsal is up. The scale bar in D corresponds to 100 μm. Wild-type

embryos, n = 19 (includes *tcf21*-/+ and or *nkx2.5*-/+ embryos), *tcf21*-/- embryos n

= 8 (includes *nkx2.5*-/+ embryos); *nkx2.5*-/- embryos (includes *tcf21*-/+ embryos),

n = 5; *tcf21*-/-; *nkx2.5*-/- embryos, n = 3. *tie1* signal is shown only when

colocalizing with mCherry, as detected using a custom-written imageJ macro

(Data S3).

Table S1. Formation of the hypobranchial artery (HA) requires tcf21+ cells.

genotype	5 dpf		
	HA completely formed	HA partially formed	HA absent
control (n=2)	100 %	0 %	0 %
tcf21+ cell ablated embryos (n=9)	0 %	33 %	67 %

Table S2. Formation of the hypobranchial artery (HA) requires Tcf21 and Nkx2.5 activities.

genotype	72 hpf			96 hpf		
	HA completely formed	HA partially formed	HA absent	HA completely formed	HA partially formed	HA absent
wild type (72 hpf, n=18) (96 hpf, n=25)	82 %	18 %	0 %	100 %	0 %	0 %
tcf21-/- (72 hpf, n=10) (96 hpf, n=26)	0 %	80 %	20 %	12 %	69 %	19 %
nkx2.5-/- (72 hpf, n=11) (96 hpf, n=19)	100%	0 %	0 %	100 %	0 %	0 %
tcf21-/-; nkx2.5-/- (72 hpf, n=5) (96 hpf, n=15)	0%	40 %	60 %	0 %	67 %	33 %

Supplemental Experimental Procedures

Zebrafish Strains

Published transgenic lines used in this study were: *Tg(tcf21:DsRed2)*[pd37] [S1], *Tg(tcf21:CreER)*[pd42] [S1], *Tg(myl7:EGFP)*[twu26],[S2] *Tg(tcf21:mCherry-NTR)*[pd108] [S3], *Tg(nkx2.5:ZsYellow)* [S4], *Tg(α-actin:GFP)* [S5], *Tg(cdh5:Gal4FF)* [S6], *Tg(flk:GFP)* [S7], *Tg(flk:ras-mCherry)* [S8], *Tg(flt1:YFP)* [S9], *Tg(bactin2:loxP-DsRed-STOP-loxP-EGFP)* [S10], *Tg(sox10:GFP)* [S11]. Transgenic embryos were identified by fluorescent protein fluorescence, transgenesis marker expression in the eye (*Tg(tcf21:CreER)*[pd42]) or PCR-amplification (*Tg(cdh5:Gal4FF)*).

PCR amplification was performed using the following primers:

tcf21[D236] mutant genotyping primers:

Outer PCR primers: 5'-CTGCTAGCAACAGCATATCCATC-3' and 5'-CCTCAGAGTACAAGTGGTG-3'

Nested PCR primers (using product of outer PCR as template) were sometimes used: 5'-CGTCCAGTCAGAGAACCTC-3' and 5'-CGAATCGGAAAACCAAAATGAAT-3'

In some cases *tcf21* genotyping results were further corroborated by the presence or absence of an amplicon using primers 5'-CGTCCAGTCAGAGAACCTC-3' and 5-CCTCTTTCCTGTACATTCTGAC-3', which should only amplify from the wild-type locus.

nkx2.5 mutant genotyping primers:

Primers: 5'-CAAACTCACCTCCACACAGG -3' and 5'-TTACCATCCCGAACCAAAAC-3'

Genotyping for *nkx2.5* mutants in the presence of *nkx2.5:ZsYellow* was accomplished using two protocols:

Both protocols used:

Outer PCR primers: 5'-CTATTAACTTCAGTGCTTCAGGC-3' and 5'-TGTTGTAAGTGGACGTGTCTC-3'

Protocol 1 used:

First nested PCR primers (using product of outer PCR as template): 5'-CTAGAAATGGACTATGTTAAAGACGC-3' and 5'-CAGACACGGTTTACCATCC-3'

Second nested PCR primers (using product of first nested PCR as template): 5'-CTAGAAATGGACTATGTTAAAGACGC-3' and 5'-TTACCATCCCGAACCAAAAC-3'

Protocol 2 used:

Only one set of nested PCR primers (using product of outer PCR as template):

5'-TGATTAATTTTTACCGGTGGTC–3' and 5'-CAGACACGGTTTACCATCC–3'

Tg(cdh5:Gal4FF) genotyping primers:

Primers: 5'-ACAGTGTGTTTGCATCATTG-3' and 5'-AGTAGCGACACTCCCAGTTG-3'.

Generation of *tcf21*[D236] Mutant Strain

For the generation of the *tcf21* mutant, we used TALEN-mediated genome
editing as described [S12]. The TALEN binding sites in exon 1 of *tcf21* were:
TAL1, 5'-TCTCCAGCCAACATGT-3; TAL2, 5'-CGATGTGGATGAATTTCACGA-
3'. Editing events were scored with the *tcf21* genotyping primers described
above. The isolated *tcf21* mutant deletes 236 base pairs. This deletion
encompasses most of the N-terminal sequence and part of the basic domain of
the basic helix-loop-helix region of Tcf21 and results in a frame shift in the
reading frame of *tcf21* (supplementary Fig. 2a). Therefore, the *tcf21*[D236] mutant is
likely an amorph.

Image analysis

For the segmentation of the movies of the *nkx2.5:ZsYellow*; *tcf21:mCherry-NTR*
embryos, we used intensity thresholding in ImageJ (NIH) to create a binary mask
for the red and green channels. To extract the voxels which contain signal from
the red and green channel (*tcf21+*/*nkx2.5+* tissue), we multiplied the mask for the
red channel with the mask for the green channel. This mask is referred to as the
mask for the red and green channel overlap. To extract the voxels that contain
signal from the red channel only (*tcf21+* tissue), we subtracted the mask for the
red and green channel overlap from the mask for the red channel. To extract the
voxels that contain signal from the green channel only (*nkx2.5+* tissue), we
subtracted the mask for the red and green channel overlap from the mask for the

green channel. These three masks – the mask for the red channel only, the mask for the green channel only and the mask for the red and green channel overlap – were sum projected and merged with DIC images and pseudo-colored to highlight the *tcf21*-only expressing cells, the *nkx2.5*-only expressing cells and the *tcf21*; *nkx2.5* co-expressing cells. Note that the intensities in these merged and sum-projected movies do not reflect fluorescence intensities but rather the amount of tissue expressing *tcf21* only, *nkx2.5* only and both *tcf21* and *nkx2.5*. This analysis was automated using a custom-written script in imageJ (NIH) (Data S1).

To segment confocal stacks of embryos expressing the *nkx2.5:ZsYellow* and *flk:mCherry* transgenes to show only endothelial transgene expression, we used intensity thresholding in ImageJ (NIH) to create a binary mask for the red channel (*flk:mCherry*). To retain only the values for voxels in the green channel which contain signal in the red channel (retaining only *nkx2.5:ZsYellow* values from *flk+* tissue), we multiplied the mask for the red channel by the green channel to create an endothelial-only thresholded version of the green channel stack. We then generated maximum projections of the red channel stack and the endothelial-only green channel stack, and merged the two projections to create single images (Figure 4B, F, J and N). This analysis was automated using a custom-written script in imageJ (NIH) (Data S2). Note that images generated with this macro were used for presentation purposes only and that the quantification of the contribution of *nkx2.5+* cells to the PAAs 3 to 6 in the different genetic

scenarios depicted in Figure 4Q was conducted using the original confocal stacks.

To segment confocal stacks of *tcf21:mCherry-NTR* embryos stained for mCherry protein and *tie1* RNA as described below, we used intensity thresholding in ImageJ (NIH) to create a binary mask for the mCherry fluorescence channel. To retain only the values for voxels in the mCherry fluorescence channel which contain signal in the *tie1* fluorescence channel, we multiplied the mask for the mCherry fluorescence channel by the *tie1* fluorescence channel to create an *tcf21+*-cell only thresholded version of the *tie1* fluorescence channel stack. We then generated sum projections of the mCherry fluorescence channel stack and the *tie1* fluorescence channel stack, and merged the two projections to create single images (Figure S3). This analysis was automated using a custom-written script in imageJ (NIH) (Data S3).

Antibodies, Stainings and *in situ* probes

For the generation of the sheep anti-mCherry antibody, N-terminally His-tagged mCherry was overexpressed in E. coli, purified and sent for custom antibody production in sheep (Covance). Sheep anti-mCherry antiserum was affinity purified using the AminoLink Plus Coupling Kit (ThermoScientific). For the generation of the rabbit anti-Cdh5 antibody, a custom affinity purified antibody was generated using genetic immunization in rabbits (amino acids 262 to 371 of zebrafish Cdh5) (SDIX, now OriGene Company).

For antibody stainings, antibodies were used against GFP (rabbit anti-GFP, 1:1000 Torrey Pines and goat anti-GFP, 1:1000 [S13]), mCherry (sheep anti-mCherry 1:1000, this study), ZsYellow (rabbit anti-RCFP, 1:1000 Clonetech), myosin heavy chain (MHC) (mouse anti-MHC/MF20, 1:100 DSHB), zn-8 (1:100) [S14] and Cdh5 (rabbit anti-Cdh5, 1:1000, this study) and were detected with donkey anti-rabbit-Alexa488 (1:500, Jackson ImmunoResearch), donkey anti-rabbit-Cy3 (1:500, Jackson ImmunoResearch), donkey anti-sheep-Alexa488 (1:500, Jackson ImmunoResearch), donkey anti-sheep-Cy3 (1:500, Jackson ImmunoResearch), donkey anti-mouse-Alexa488 (1:500, Jackson ImmunoResearch), donkey anti-mouse-Cy3 (1:500, Jackson ImmunoResearch), donkey anti-goat-Alexa488 (1:500, Jackson ImmunoResearch), donkey anti-mouse-Alexa647 (1:2000, Jackson ImmunoResearch) or donkey anti-goat-Cy3 (1:500, Jackson ImmunoResearch). Alcian blue staining was performed as described in [S15]. RNA probe synthesis and in situ hybridization was performed as previously described [S16]. RNA probes against *tcf21*, *pitx2c* and *tie1* were labeled with DIG (Roche) and detected with anti-DIG antibody coupled to alkaline phosphatase (1:5000, Roche) and NBT/BCIP (Roche) or anti-DIG antibody coupled to horseradish peroxidase (1:1000, Roche) and Cy3-tyramide signal amplification (Perkin Elmer). For stainings against *tie1*, the anti-DIG-HRP signal was amplified using DNP-tyramide (Perkin Elmer), followed by incubation with anti-DNP antibody coupled to horseradish peroxidase (1:1000, Perkin Elmer) and then Cy3-tyramide signal amplification (Perkin Elmer).

Supplemental References

S1.   Kikuchi, K., Gupta, V., Wang, J., Holdway, J. E., Wills, A. A., Fang, Y., and
       Poss, K. D. (2011). tcf21+ epicardial cells adopt non-myocardial fates
       during zebrafish heart development and regeneration. Development *138*,
       2895–2902.

S2.   Huang, C.-J., Tu, C.-T., Hsiao, C.-D., Hsieh, F.-J., and Tsai, H.-J. (2003).
       Germ-line transmission of a myocardium-specific GFP transgene reveals
       critical regulatory elements in the cardiac myosin light chain 2 promoter of
       zebrafish. Dev Dyn *228*, 30–40.

S3.   Wang, J., Cao, J., Dickson, A. L., and Poss, K. D. (2015). Epicardial
       regeneration is guided by cardiac outflow tract and Hedgehog signalling.
       Nature.

S4.   Zhou, Y., Cashman, T. J., Nevis, K. R., Obregon, P., Carney, S. A., Liu, Y.,
       Gu, A., Mosimann, C., Sondalle, S., Peterson, R. E., et al. (2011). Latent
       TGF-β binding protein 3 identifies a second heart field in zebrafish. Nature
       474, 645–648.

S5.   Higashijima, S., Okamoto, H., Ueno, N., Hotta, Y., and Eguchi, G. (1997).
       High-frequency generation of transgenic zebrafish which reliably express
       GFP in whole muscles or the whole body by using promoters of zebrafish
       origin. Dev Biol *192*, 289–299.

S6.   Bussmann, J., Wolfe, S. A., and Siekmann, A. F. (2011). Arterial-venous network formation during brain vascularization involves hemodynamic regulation of chemokine signaling. Development *138*, 1717–1726.

S7.   Choi, J., Dong, L., Ahn, J., Dao, D., Hammerschmidt, M., and Chen, J.-N. (2007). FoxH1 negatively modulates flk1 gene expression and vascular formation in zebrafish. Dev Biol *304*, 735–744.

S8.   Chi, N. C., Shaw, R. M., De Val, S., Kang, G., Jan, L. Y., Black, B. L., and Stainier, D. Y. R. (2008). Foxn4 directly regulates tbx2b expression and atrioventricular canal formation. Genes Dev *22*, 734–739.

S9.   Hogan, B. M., Bos, F. L., Bussmann, J., Witte, M., Chi, N. C., Duckers, H. J., and Schulte-Merker, S. (2009). ccbe1 is required for embryonic lymphangiogenesis and venous sprouting. Nat Genet *41*, 396–398.

S10. Kikuchi, K., Holdway, J. E., Werdich, A. A., Anderson, R. M., Fang, Y., Egnaczyk, G. F., Evans, T., Macrae, C. A., Stainier, D. Y. R., and Poss, K. D. (2010). Primary contribution to zebrafish heart regeneration by gata4(+) cardiomyocytes. Nature *464*, 601–605.

S11. Carney, T. J., Dutton, K. A., Greenhill, E., Delfino-Machin, M., Dufourcq, P., Blader, P., and Kelsh, R. N. (2006). A direct role for Sox10 in specification of neural crest-derived sensory neurons. Development *133*, 4619–4630.

S12. Dahlem, T. J., Hoshijima, K., Jurynec, M. J., Gunther, D., Starker, C. G., Locke, A. S., Weis, A. M., Voytas, D. F., and Grunwald, D. J. (2012).

Simple Methods for Generating and Detecting Locus-Specific Mutations Induced with TALENs in the Zebrafish Genome. PLoS Genet *8*, e1002861.

S13. Venkiteswaran, G., Lewellis, S. W., Wang, J., Reynolds, E., Nicholson, C., and Knaut, H. (2013). Generation and Dynamics of an Endogenous, Self-Generated Signaling Gradient across a Migrating Tissue. Cell *155*, 674–687.

S14. Trevarrow, B., Marks, D. L., and Kimmel, C. B. (1990). Organization of hindbrain segments in the zebrafish embryo. Neuron *4*, 669–679.

S15. Walker, M., and Kimmel, C. (2007). A two-color acid-free cartilage and bone stain for zebrafish larvae. Biotech Histochem *82*, 23–28.

S16. Thisse, C., and Thisse, B. (2008). High-resolution in situ hybridization to whole-mount zebrafish embryos. Nature Protocols *3*, 59–69.